ISSN 0036-0244, Russian Journal of Physical Chemistry A, 2019, Vol. 93, No. 2, pp. 359–368. © Pleiades Publishing, Ltd., 2019.

COLLOID CHEMISTRY AND ELECTROCHEMISTRY

# Investigation of Electrochemical Characterization of the Protective Film Formed by the Novel Schiff's Base on the Carbon Steel Surface in Acid Media: Temperature Effects and Thermodynamic Parameters[1]

**Duygu Ataş[a] and Emel Bayol[a,*]**

[a] *Niğde Ömer Halisdemir University, Faculty of Science and Arts, Department of Chemistry, Niğde, 51240 Turkey*

**e-mail: emelbayol@ohu.edu.tr*

Received February 22, 2018

**Abstract**—Two Schiff bases containing different functional groups were synthesized. Their inhibition performance and adsorption behavior on carbon steel corrosion behavior in acidic media were investigated using electrochemical techniques at different concentrations and temperatures. Results showed that the inhibitors inhibited carbon steel corrosion in acid solution and indicated that the inhibition efficiencies were enhanced with an increase in concentration of inhibitor. Polarization studies showed that the inhibitors behave as mixed type of inhibitors. The adsorption of the inhibitors on a carbon steel surface obeys Langmuir's adsorption isotherm. The values of activation energy and the thermodynamic parameters, such as $K_{ads}$, $\Delta G^{\circ}_{ads}$, $\Delta H^{\circ}_{ads}$, and $\Delta S^{\circ}_{ads}$ were calculated and discussed. The surface adsorbed film was characterized by atomic force microscopy.

*Keywords:* carbon steel, acid corrosion, Schiff bases, electrochemical measurements, thermodynamic parameters

**DOI:** 10.1134/S0036024419020080

## INTRODUCTION

Ferrous and its alloys are commonly used in a variety of industrial applications such as chemical processing, petroleum production and refining, construction and metal processing equipment due to its low cost and excellent mechanical properties [1, 2]. HCl solution is widely used in industry in many processes, such as removal scale and salt deposits or mill scales formed during manufacturing, pickling, industrial acid cleaning and oil refinery equipment. However, the main problem of using metals is their dissolution in acidic solutions [3–7]. The use of inhibitors is one of the most convenient methods for protection against corrosion especially in acidic media [8–13]. The choice of the inhibitors depends on whether they could be synthesized conventionally from relatively cheap raw materials or on the presence of either >C=N group that provide electron density to the aromatic ring or an electronegative atoms such as nitrogen and oxygen in a relatively long chain compounds [14–18]. Schiff bases are condensation products of an amine and a ketone/aldehyde. Schiff base inhibitors have been reported as good corrosion inhibitors for steel, copper and aluminum [19–23].

In this study, two different Schiff bases were synthesized and their structure was characterized by the $^1$H-NMR, FT-IR, and UV–Vis spectroscopic techniques. These inhibitors contained a benzene ring conjugated with imine group (C=N, Schiff base), a benzene ring with an electron-releasing hydroxyl (–OH) group, and both hydroxyl (–OH) and methoxy groups ($-OCH_3$) (Table 1). The effects of concentrations, temperatures and molecular structures on the inhibition efficiencies of the Schiff base in acidic solution have been studied.

## EXPERIMENTAL

### *Materials*

Electrochemical measurements were conducted in a conventional three-electrode thermostatted cell. Platinum foils of 1 × 1 cm as counter electrode and Ag/AgCl, KCl (3 M) as the reference electrode have been used in the electrochemical studies. The working electrode was prepared from a cylindrical carbon steel bar. The corrosion tests were performed on carbon steel rod with a composition (in wt %) C = 0.712, Al = 0.018, Si = 0.244, P = 0.024, S = 0.022, Ti = 0.008, V = 0.021, Cr = 0.010, Mn = 0.688, Co = 0.014, Ni = 0.045, Cu = 0.092, Nb = 0.031, Mo = 0.002, Sn = 0.004, and Fe = 98.064. The electrode was embedded in polyester so that only its surface (0.5024 cm$^2$) was allowed to contact with the aggressive solutions. The electrodes were mechanically abraded with a series of emery papers (200, 800, and 1200 grit) and were rinsed in acetone and double distilled water before immer-

[1] The article is published in the original.

**Table 1.** Molecular structure and analytical data of Schiff bases

| The names and structures | Analytical data |
|---|---|
| 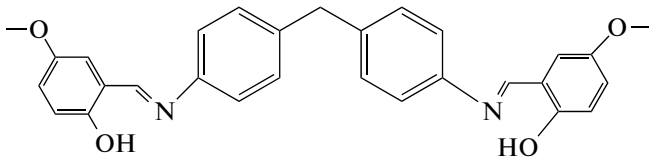 <br>2,2'-(1*E*,1'*E*)-(4,4'-methylenebis(4,1-phenylene)bis(azan-1-yl-1-ylidene))bis(methan-1-yl-1-ylidene)bis(4-methoxyphenol) (DfMeO) | mp: 217 °C;<br>$^1$H NMR/ $CDCl_3$/d, ppm: 8.60 (HC=N);<br>IR (KBr)/ν =1622 $cm^{-1}$;<br>UV ($CH_2Cl_2$)/$\lambda_{max}$ = 370 nm |
| 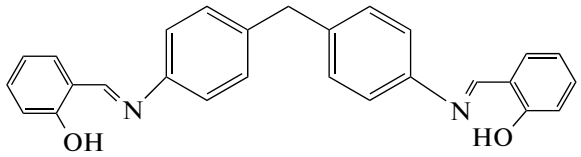 <br>2,2'-(1*E*,1'*E*)-(4,4'-methylenebis(4,1-phenylene)bis(azan-1-yl-1-ylidene))bis(methan-1-yl-1-ylidene)diphenol (DfS) | mp: 210 °C;<br>$^1$H NMR/ $CDCl_3$/d, ppm: 8.64 (HC=N);<br>IR (KBr)/ν =1614 $cm^{-1}$;<br>UV ($CH_2Cl_2$)/$\lambda_{max}$ = 346 nm |

sion in the test solution. The concentration range of inhibitors employed was $1.0 \times 10^{-4}$–$1.0 \times 10^{-3}$ M. The three-electrode cell was thermostatted with a wear jacket at various temperatures (298, 308, 318, and 328 K). All electrochemical measurements were carried out using a CHI 660B computer-controlled electrochemical analyzer.

### *Synthesis of Inhibitors*

The Schiff base compounds used were synthesized by condensation of 4,4'-diaminodiphenylmethane (10 mmol) with the corresponding aldehydes (20 mmol) in methanolic solution. The aldehyde compounds used were 2-hydroxybenzaldehyde and 2-hydroxy-5-methoxybenzaldehyde. All chemicals were purchased from Merck and were used without further purification. The structures of these products were confirmed by $^1$H-NMR and FT-IR, UV–Vis spectroscopy. The molecular structure and analytical data of the inhibitors are given in Table 1.

### *Electrochemical Studies*

The working electrode was first immersed in the test solution for 1 h to gain a steady state open circuit potential. Electrochemical impedance (EIS) measurements were performed at an open circuit potential in the frequency range from $1 \times 10^5$ to $5 \times 10^{-3}$ Hz, with an AC signal amplitude of 5 mV. After measuring the open circuit potential ($E_{corr}$), the polarization curves were obtained from potentiodynamic polarization measurements at cathodic potential (−0.250 V) and at (+0.250 V) anodic potential (Ag/AgCl) starting from the corrosion potential at a scan rate of 1.0 mV $s^{-1}$. The cathodic Tafel slope ($\beta_c$) and corrosion current densities ($i_{corr}$) were obtained from the cathodic polarization curves.

### *Surface Morphology*

The morphology of the corroded surface was studied after 120 h of exposure time in 1.0 M HCl and $1.0 \times 10^{-3}$ M of Schiff bases by AFM technique. AFM measurements were performed using a Veeco Multimode 8 Nanoscope 3D model AFM.

## RESULTS AND DISCUSSION

### *Electrochemical Measurements*

Polarization curves of carbon steel in 1.0 M HCl without and with $1.0 \times 10^{-3}$ M Schiff bases at different temperature are presented in Fig. 1. Similar curves were obtained for other concentration (not shown).

The corrosion current density ($i_{corr}$) was calculated from the cathodic polarization curves and the inhibition efficiency was calculated from the following equation [8]:

$$IE, \% = \left( \frac{i_{corr} - i^{\circ}_{corr}}{i_{corr}} \right) \times 100, \quad (1)$$

where $i_{corr}$ and $i^{\circ}_{corr}$ represent the corrosion current densities in the absence and presence of the inhibitor respectively.

The cathodic Tafel slopes ($\beta_c$), corrosion potential ($E_{corr}$), corrosion current density ($i_{corr}$) and the inhibition efficiency (*IE*, %) data are listed in Table 2. As it can be seen from Table 2, corrosion current density increases with temperature in an uninhibited solution. This behavior can be related to that increasing temperature accelerates all the other processes involved in corrosion such as electrochemical reactions, chemical

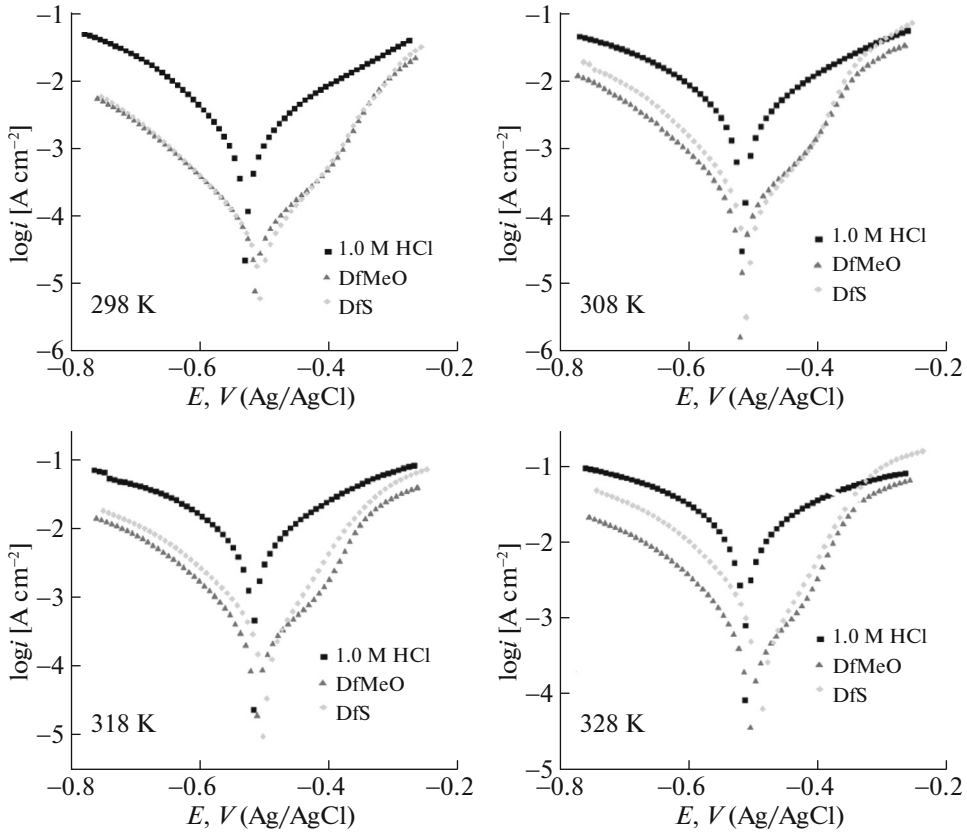


**Fig. 1.** Potentiodynamic polarization curves of carbon steel in 1.0 M HCl solution in the absence and presence of $1.0 \times 10^{-3}$ M Schiff bases at 298–328 K.

reactions and transfer process of reactive species to the metal surface [24]. Both anodic and cathodic current densities in the presence of inhibitor were found to be lower compared to those obtained without inhibitor. As observed, the inhibition efficiency increases with the increase in concentration of each inhibitor. These results indicate that the inhibitors are efficient in the temperature range studied.

The cathodic Tafel constant values ($\beta_c$) did not change significantly at 298 K, which shows that the hydrogen evolution mechanism has not been affected by the addition of Schiff bases. The curves give rise to parallel Tafel lines which indicate that hydrogen evolution reaction is activation controlled, and the inhibiting action occurred by simple blocking of the available cathodic sites on the metal surface, which lead to a decrease in the actual surface area available for hydrogen evolution and lowered the dissolution rate with increasing inhibitors concentration. As the temperature increases, the cathodic Tafel constant values increase in Table 2. This increase may be greater in the absence inhibitor than in the presence inhibitor since the reduction of hydrogen ions on the bare metal surface is easier than the metal surface coated with the inhibitor molecules. Similar findings have been reported in the literature [25–28].

Only as the change in $E_{corr}$ value was more than 85 mV, a compound could be recognized as an anodic or a cathodic type inhibitor. The largest displacement of $E_{corr}$ values was about 37 mV. Therefore, inhibitors might act as a mixed type inhibitor. The inhibition efficiency has slightly lower at concentrations $\leq 5.0 \times 10^{-4}$ M when the temperature has increased from 298 to 328 K. The drop in inhibition efficiency at low concentration is probably due to desorption of some adsorbed molecule on the metal surface at higher temperatures [29, 30]. This shows a weak adsorption interaction between the metal surface and the inhibitor. The inhibition efficiency remains high and almost constant with the increase of temperature at $7.5 \times 10^{-3}$ and $1.0 \times 10^{-3}$ M. With high inhibitor concentration a compact and coherent inhibitor layer was formed on the carbon steel which reduces chemical attack on the metal, and implying that high degree of surface coverage was kept at even high temperatures [6, 31–35].

Electrochemical impedance spectroscopy (EIS) is an in situ, nondestructive, rapid and convenient technique for evaluating the metal surface coverage [36–39]. Impedance measurements of carbon steel in 1.0 M HCl at 298 K was performed in the absence and presence of different concentrations of Schiff base

**Table 2.** Corrosion parameters obtained from polarization curves of carbon steel in 1.0 M HCl in the absence and presence of different concentrations ($c$) of Schiff bases at different temperatures

| $C$, × $10^{-4}$ M | DfMeO | | | | DfS | | | |
|---|---|---|---|---|---|---|---|---|
| | $-E_{corr}$, mV | $-\beta_c$, mV dec$^{-1}$ | $i_{corr}$, μA/cm$^2$ | $IE$, % | $-E_{corr}$, mV | $-\beta_c$, mV dec$^{-1}$ | $i_{corr}$, μA/cm$^2$ | $IE$, % |
| 2 | 298 K | | | | | | | |
| 0 | 0.530 | 130 | 1273 | | 0.530 | 130 | 1273 | |
| 1.0 | 0.517 | 117 | 286 | 78 | 0.521 | 124 | 354 | 72 |
| 2.5 | 0.525 | 121 | 216 | 83 | 0.519 | 113 | 218 | 83 |
| 5.0 | 0.493 | 124 | 107 | 92 | 0.505 | 107 | 75 | 94 |
| 7.5 | 0.494 | 130 | 68 | 95 | 0.515 | 108 | 73 | 94 |
| 10 | 0.510 | 114 | 63 | 95 | 0.504 | 107 | 50 | 96 |
| | 308 K | | | | | | | |
| 0 | 0.521 | 214 | 3726 | | 0.521 | 214 | 3726 | |
| 1.0 | 0.514 | 156 | 1495 | 60 | 0.519 | 148 | 1560 | 58 |
| 2.5 | 0.513 | 143 | 748 | 80 | 0.512 | 117 | 607 | 84 |
| 5.0 | 0.509 | 124 | 322 | 91 | 0.514 | 134 | 705 | 81 |
| 7.5 | 0.506 | 123 | 159 | 96 | 0.509 | 122 | 331 | 91 |
| 10 | 0.524 | 121 | 192 | 95 | 0.515 | 109 | 234 | 94 |
| | 318 K | | | | | | | |
| 0 | 0.517 | 240 | 7677 | | 0.517 | 240 | 7677 | |
| 1.0 | 0.511 | 169 | 3790 | 51 | 0.514 | 172 | 4670 | 39 |
| 2.5 | 0.507 | 168 | 1689 | 78 | 0.508 | 225 | 2667 | 65 |
| 5.0 | 0.506 | 170 | 1247 | 84 | 0.509 | 180 | 2118 | 72 |
| 7.5 | 0.508 | 124 | 332 | 96 | 0.505 | 178 | 1356 | 82 |
| 10 | 0.514 | 130 | 371 | 95 | 0.503 | 133 | 514 | 93 |
| | 328 K | | | | | | | |
| 0 | 0.512 | 290 | 16170 | | 0.512 | 290 | 16170 | |
| 1.0 | 0.502 | 240 | 9773 | 40 | 0.510 | 310 | 9891 | 39 |
| 2.5 | 0.501 | 216 | 4510 | 72 | 0.503 | 238 | 9597 | 41 |
| 5.0 | 0.497 | 222 | 2867 | 82 | 0.498 | 226 | 4438 | 73 |
| 7.5 | 0.500 | 167 | 1851 | 89 | 0.497 | 198 | 2672 | 84 |
| 10 | 0.506 | 150 | 842 | 95 | 0.495 | 154 | 2061 | 87 |

derivatives. The representative Nyquist and Bode plots after 1 h exposure are given in Fig. 2.

The experimental data were fitted to the proposed equivalent circuit in Figs. 3a, 3b using Zview program [40]. The percentage inhibition efficiency, $IE$ (%), was calculated by using the following expression:

$$IE, \% = \left( \frac{R_p - R_p^\circ}{R_p} \right) \times 100, \quad (2)$$

$$\theta = \left( \frac{R_p - R_p^\circ}{R_p} \right), \quad (3)$$

where $R_p$ and $R_p^\circ$ are the polarization resistance of the electrode with and without inhibitor respectively. The corresponding corrosion parameters for each system are collected in Table 3.

As can be seen from Fig. 2, the Nyquist plot of carbon steel in HCl solution does not yield perfect semicircle as expected from the theory of electrochemical impedance spectroscopy. The deviation from ideal semicircle is generally attributed to the frequency dispersion as a result of surface roughness, impurities, dislocations, grain boundaries, adsorption of inhibitors, formation of porous layers and in homogenates of the electrode surface [41–43]. The experimental impedance data were fitted according to the electrical equivalent circuit diagram given in Fig. 3a in order to model the uninhibited carbon steel/solution interface.

The difference in real impedance at lower and higher frequencies is considered as polarization resis-

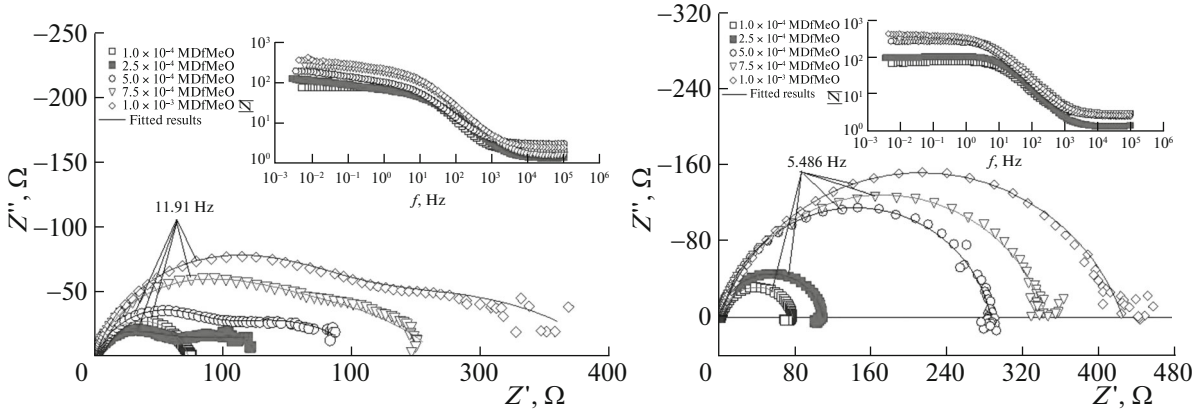


**Fig. 2.** Nyquist and Bode plots of carbon steel in 1.0 M HCl in the presence of different concentration of DfMeO and DfS at 298 K.

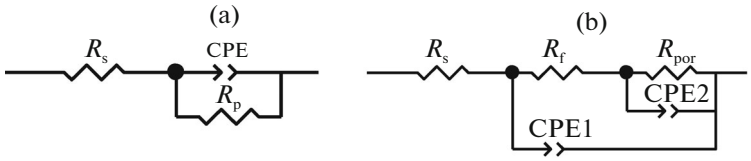


**Fig. 3.** Equivalent circuit used to fit impedance spectra in the absence (a) and presence (b) of Schiff bases; (a) $R_p = R_{ct} + R_d + R_a$, (b) $R_p = R_f + R_{por}$ ($R_{por} = R_{ct} + R_d + R_a$) for the diagrams ($R_s$) solution resistance, ($R_{ct}$) charge transfer resistance, ($R_d$) diffuse layer resistance, ($R_a$) resistance of accumulated species at metal/solution interface, ($R_f$) film resistance, ($R_{por}$) pore resistance, ($CPE_1$) film capacitance, (CPE and $CPE_2$) double layer capacitance.

tance ($R_p$). The polarization resistance includes charge transfer resistance ($R_{ct}$) which corresponds to the resistance between the metal/outer Helmholtz plane and diffuse layer resistance ($R_d$) containing corrosion products and the accumulated species ($R_a$) on the metal surface of the semiellipse model that has been reported by Erbil et al. [44, 45].

Nyquist plots showed two slightly disturbed capacitive loops (two time constant); at high and low frequency regions in the presence of the Schiff bases. The first loop that appeared at high frequency region is attributed to the $R_{ct}$, the $R_d$ and the $R_a$. Where, the sum of these resistances is known as pore resistance ($R_{por}$). The second loop is attributed to the film resistance and to all of the other accumulated species such as corrosion products, inhibitor molecules, etc. that agrees with literature [38, 41].

**Table 3.** Polarization resistance and inhibition efficiency values of carbon steel in 1.0 M HCl solution in the absence and presence of various concentrations ($c$) Schiff bases

| $C$, $\times 10^{-4}$ M | DfMeO | | | DfS | | |
|---|---|---|---|---|---|---|
| | $-E_{corr}$, V | $R_p$, Ω | $IE$, % | $-E_{corr}$, V | $R_p$, Ω | $IE$, % |
| 0 | 0.535 | 27 | | 0.535 | 27 | |
| 1.0 | 0.518 | 72 | 62 | 0.522 | 76 | 64 |
| 2.5 | 0.521 | 221 | 88 | 0.520 | 109 | 75 |
| 5.0 | 0.491 | 207 | 87 | 0.504 | 285 | 90 |
| 7.5 | 0.487 | 268 | 90 | 0.514 | 342 | 92 |
| 10 | 0.507 | 400 | 93 | 0.504 | 423 | 94 |

The electrochemical impedance results clearly indicates that the increase in the concentration of the two Schiff bases has increased polarization resistance after 1 h the immersion of the electrode in 1.0 M HCl solution, therefore a larger diameter of the semicircle was observed in Nyquist plots (Fig. 2 and Table 3). As it is seen from Table 3, the polarization resistance value of the blank was 27 Ω and has increased when inhibitors was added. The $R_p$ values at highest concentrations of DfS and DfMeO were 423 and 400 Ω, respectively.

Nyquist and Bode plots for carbon steel solutions containing $1.0 \times 10^{-3}$ M Schiff bases at different temperature are shown in Fig. 4. Similar curves were obtained for other concentration (not shown).

Table 4 collects the values of corrosion parameters of mild steel at different concentrations of inhibitors determined by impedance measurements at various temperatures (308–328 K).

The efficiency of Schiff bases have slightly decreased for the solutions at lower concentrations while the efficiency in concentrated solutions have remained almost unchanged with the rise of temperature (Table 4). This may indicate a strong inhibitor–metal bond.

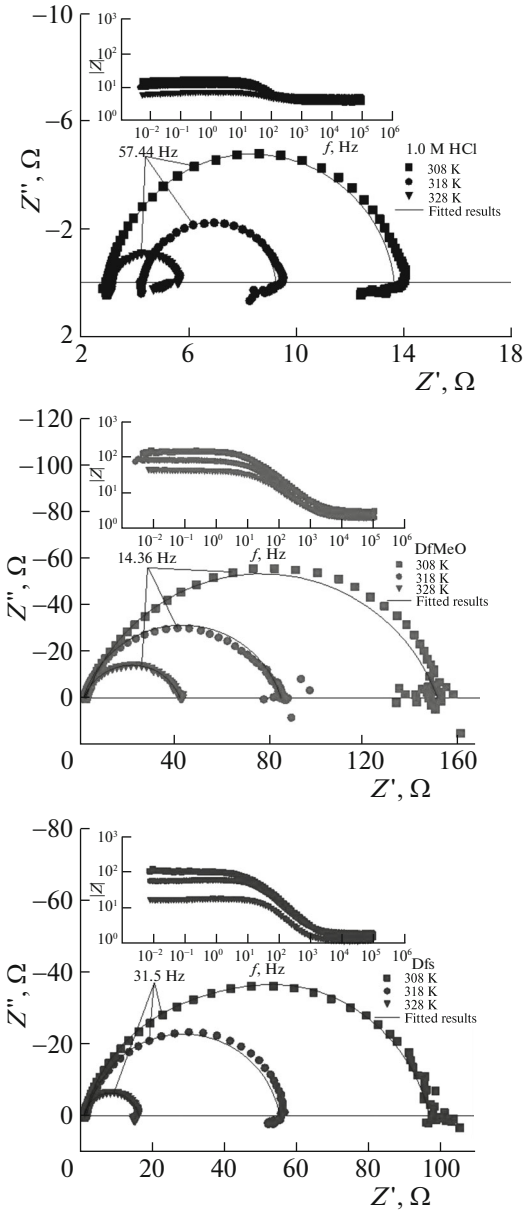


**Fig. 4.** Nyquist and Bode plots of carbon steel in 1.0 M HCl solution in absence and presence of $1.0 \times 10^3$ M inhibitors at different temperature.

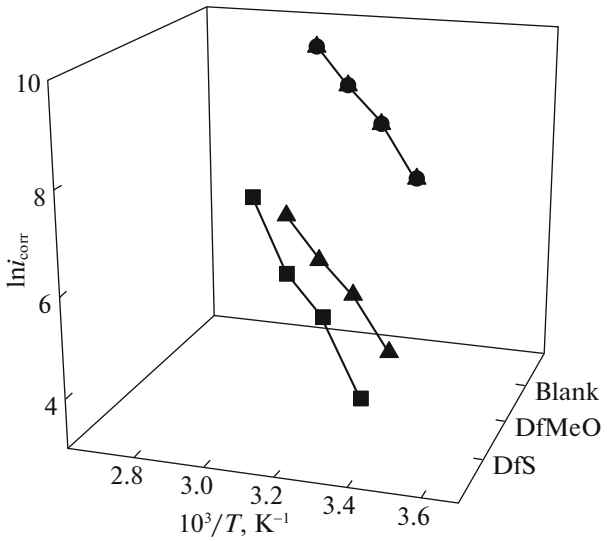


**Fig. 5.** Arrhenius plots of ln $i_{corr}$ vs. $1/T$ for carbon steel in 1.0 M HCl in the absence and presence of inhibitors.

### *Thermodynamic Activation Parameters*

A kinetic model is another useful tool to explain the mechanism of corrosion inhibition for the inhibitor. The apparent activation energy of the corrosion reaction was determined by using Arrhenius plots. Arrhenius equation could be written as [46, 47]:

$$\ln i_{corr} = \ln A - \frac{E_a}{RT}, \quad (4)$$

where $E_a$ represents the apparent activation energy, $R$ is the gas constant, $A$ is the preexponential factor, and $i_{corr}$ is the corrosion rate obtained from the potentiodynamic polarization method. Ploting ln $i_{corr}$ vs. $1/T$, the values of $E_a$ can be calculated from the slopes of straight lines obtained from Fig. 5. The values of $E_a$ for the compound studied are listed in Table 5.

The $E_a$ value for the carbon steel corrosion in an uninhibited medium is 67.97 kJ mol$^{-1}$. It can also be seen that at lower concentration of inhibitors the activation energy has increased compared to the free acid solution. This increase could be attributed to the adsorption–desorption equilibrium shift towards desorption with the increase of temperature and thus indicating a physical adsorption mechanism [48–50]. At highest concentration, activation energy did not change or even lowered for all inhibitors. This results shows that, lower concentrations physisorption of Schiff bases occur while at higher concentrations strong physisorption is observed [51, 52].

### *Adsorption Isotherm and Thermodynamic Adsorption Parameters*

Thermodynamic adsorption parameters are the standard free energy of adsorption ($\Delta G^\circ_{ads}$), the standard heat of adsorption ($\Delta H^\circ_{ads}$), and the standard entropy of adsorption ($\Delta S^\circ_{ads}$). The increase in efficiency of inhibition of the carbon steel corrosion in 1.0 M HCl with increasing concentrations of Schiff bases can be explained on the basis of inhibitor adsorption. The process of adsorption of inhibitors is influenced by the chemical structures of organic compounds, the nature and surface charge of metal, the temperature, the distribution of charge in the molecule and the solution's chemical composition [22, 53]. Since adsorption isotherms can provide important clues to the nature of metal–inhibitor interaction.

The adsorption mechanism of the examined Schiff bases on the carbon steel surface was determined by

**Table 4.** Corrosion parameters obtained from EIS measurements of carbon steel in 1.0 M HCl solution containing various concentrations ($c$) of the Schiff bases at different temperatures

| $C$, $\times 10^{-4}$ M | DfMeO | | | DfS | | |
|---|---|---|---|---|---|---|
| | $-E_{corr}$, V | $R_p$, Ω | $IE$, % | $-E_{corr}$, V | $R_p$, Ω | $IE$, % |
| 308 K | | | | | | |
| 0 | 0.522 | 11 | — | 0.522 | 11 | — |
| 1.0 | 0.519 | 34 | 69 | 0.521 | 19 | 45 |
| 2.5 | 0.515 | 39 | 73 | 0.520 | 36 | 71 |
| 5.0 | 0.506 | 82 | 87 | 0.514 | 39 | 72 |
| 7.5 | 0.504 | 176 | 94 | 0.507 | 75 | 86 |
| 10 | 0.516 | 148 | 93 | 0.524 | 96 | 89 |
| 318 K | | | | | | |
| 0 | 0.513 | 5 | — | 0.513 | 5 | — |
| 1.0 | 0.513 | 11 | 53 | 0.515 | 8 | 40 |
| 2.5 | 0.515 | 24 | 80 | 0.509 | 12 | 60 |
| 5.0 | 0.506 | 28 | 82 | 0.511 | 16 | 68 |
| 7.5 | 0.516 | 82 | 94 | 0.505 | 26 | 81 |
| 10 | 0.516 | 83 | 94 | 0.502 | 54 | 91 |
| 328 K | | | | | | |
| 0 | 0.510 | 2.5 | — | 0.510 | 2.5 | — |
| 1.0 | 0.504 | 4 | 40 | 0.510 | 3.8 | 33 |
| 2.5 | 0.503 | 9 | 72 | 0.503 | 4.5 | 44 |
| 5.0 | 0.499 | 11 | 78 | 0.498 | 9 | 72 |
| 7.5 | 0.501 | 17 | 85 | 0.497 | 13 | 81 |
| 10 | 0.506 | 40 | 94 | 0.495 | 15 | 84 |

**Table 5.** Activation energies (kJ mol$^{-1}$) of inhibitors in 1.0 M HCl using the obtained data from potentiodynamic polarization technique

| $C$, $\times 10^{-4}$ M | DfS | DfMeO |
|---|---|---|
| 0 | 67.97 | 67.97 |
| 1.0 | 90.43 | 93.96 |
| 2.5 | 104.12 | 80.79 |
| 5.0 | 108.99 | 91.25 |
| 7.5 | 99.49 | 86.03 |
| 10 | 97.28 | 68.67 |

fitting the θ values (obtained from EIS measurements) to different adsorption isotherms such as Langmuir, Frumkin, Freundlich, Temkin and Florry–Huggins for different temperatures. The best fits were obtained for Langmuir adsorption isotherm, where the correlation coefficients for all temperatures were calculated as 0.9778 and 0.9992. According to this isotherm, θ is related to the inhibitor concentration $C_{(inh)}$ [54]:

$$\frac{C_{(inh)}}{\theta} = \frac{1}{K_{ads}} + C, \quad (5)$$

where $C_{(inh)}$ is the inhibitor concentration and $K_{ads}$ is the adsorption equilibrium constant of the adsorption process. The adsorption isotherms are plotted in Fig. 6.

The standard free energy of adsorption, $\Delta G^\circ_{ads}$ characterizes the adsorption interaction with the metal surface. The equilibrium constant for adsorption process is related to $\Delta G^\circ_{ads}$ and is calculated by following equation:

$$K_{ads} = \frac{1}{55.5}\exp\left(-\frac{\Delta G^\circ_{ads}}{RT}\right), \quad (6)$$

where 55.5 is the molar concentration of water in solution [5, 28]. The values of $\Delta G^\circ_{ads}$ is listed in Table 6.

It is generally accepted that the values of $\Delta G^\circ_{ads}$ of the order of −20 kJ mol$^{-1}$ or lower (more positive) are regarded as physisorption, the inhibition acts due to the electrostatic interactions between the charged organic molecules and the charged metal surface. On the other hand, the $\Delta G^\circ_{ads}$ value around −40 kJ mol$^{-1}$ or higher (more negative) involve chemisorptions, which is due to the charge sharing or a transfer from the inhibitor molecules to the metal surface to form a covalent bond [48, 55–58]. It is shown that the calculated negative $\Delta G^\circ_{ads}$ values, is ranging from 34.584 to 35.284 kJ mol$^{-1}$ for DfMeO and from 33.258 to 35.889 kJ mol$^{-1}$ for DfS at all the temperatures studied. The high negative value of $\Delta G^\circ_{ads}$ shows the spontaneous adsorption of inhibitors on the surface of steel and a strong interaction between the inhibitor and the surface of carbon steel [59, 60]. Thermodynamic model can be applied to the corrosion inhibition of carbon steel in the presence of Schiff bases.

The most common independent variables are $T$ and $P$, and from Gibbs equations we can obtain temperature dependences of free energy, $G$, which is expressed as

$$dG = -SdT + VdP. \quad (7)$$

At constant pressure, if we substitute for $dP = 0$ and next equation is obtained:

$$\Delta S^\circ_{ads} = -\left(\frac{\partial G}{\partial T}\right)_P. \quad (8)$$

When the values are substituted into Eq. (8), a second degree polynomial of the standard adsorption free energy versus temperature graph is obtained.

$\Delta G^\circ_{ads}$ versus $T$ values gives a mathematical relation which is expressed as follows equation for DfMeO:

$$\left(\frac{\partial G^\circ_{ads}}{\partial T}\right)_P = 1.5793T^2 - 1005.3T + 124775. \quad (9)$$

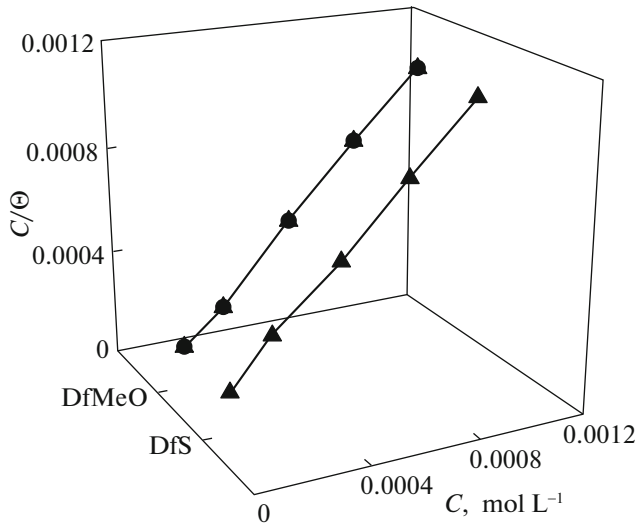


**Fig. 6.** Langmuir isotherm plots for adsorption of all the examined Schiff bases compounds on carbon steel in 1.0 M HCl at 298 K

Second order polynomial expression was obtained. By deriving expression (9) we can calculate $\Delta S^{\circ}_{ads}$ values at all study temperatures

$$\Delta S^{\circ}_{ads} = -3.1586T + 1005.3, \quad (10)$$

$\Delta H^{\circ}_{ads}$ values at all studied temperatures were calculated from the basic thermodynamic equation:

$$\Delta G^{\circ}_{ads} = \Delta H^{\circ}_{ads} - T\Delta S^{\circ}_{ads}. \quad (11)$$

The values of $\Delta H^{\circ}_{ads}$ and $\Delta S^{\circ}_{ads}$ are summarized in Table 6.

The negative $\Delta G^{\circ}_{ads}$ values did not significantly change by increasing temperatures, indicating that the adsorption is favorable and interaction seems to be strong physical.

**Table 6.** The thermodynamic parameters at different temperatures

| $T$, K | $K_{ads}$ | $-\Delta G^{\circ}_{ads}$, kJ mol$^{-1}$ | $\Delta S^{\circ}_{ads}$, J mol$^{-1}$ K$^{-1}$ | $-\Delta H^{\circ}_{ads}$, kJ mol$^{-1}$ |
|---|---|---|---|---|
| | | DfMeO | | |
| 298 | 20790 | 34.584 | 63.90 | 15.54 |
| 308 | 15337 | 34.965 | 32.30 | 25.17 |
| 318 | 11261 | 35.284 | −11.40 | 38.91 |
| 328 | 6840 | 35.033 | −30.80 | 45.14 |
| | | DfS | | |
| 298 | 15773 | 33.899 | −75.20 | 56.31 |
| 308 | 7874 | 33.258 | −32.80 | 43.36 |
| 318 | 5316 | 33.299 | −9.60 | 36.35 |
| 328 | 3906 | 33.506 | 52.0 | 16.45 |

Valuable information about the mechanism of corrosion inhibition can be provided from the values of thermodynamic parameters for the adsorption of inhibitor. In an exothermic process, physisorption is distinguished from chemisorption by the absolute value of $\Delta H^{\circ}_{ads}$. This value is lower than 40 kJ mol$^{-1}$ for the physisorption process while in the chemisorption process it approaches 100 kJ mol$^{-1}$ [23, 61]. In this work, the negative sign of $\Delta H^{\circ}_{ads}$ indicated that the adsorption of inhibitors used is exothermic. As a result, the calculated $\Delta G^{\circ}_{ads}$ and $\Delta H^{\circ}_{ads}$ values for all Schiff bases showed that the adsorption mechanism are strong physisorption [4, 5, 45].

$\Delta S^{\circ}_{ads}$ values were getting smaller by increasing temperature. This behavior may be explained as: Before the adsorption of inhibitor molecules onto steel surface, inhibitor molecules moves freely in the bulk solution (are chaotic) but as adsorption progresses, inhibitor molecules are adsorbed more orderly onto the steel surface; resulting in a decrease in entropy [30, 58, 62]. It seems that ordering caused by adsorption of DfMeO molecules override the disorder caused by the temperature effect [61]. However, $\Delta S^{\circ}_{ads}$ as values in the presence of DfS were getting bigger by increasing temperature, which mean that, an increase in disorder is due to the adsorption of only one inhibitor molecule and the desorption of more water molecules [34, 62]. The thermodynamic values obtained are the sum of adsorption of organic inhibitor molecule and desorption of water molecules [40, 51].

### *Surface Morphology*

The three dimensional (3D) AFM images of carbon steel, which were immersed in blank and containing Schiff bases after 120 h, were presented in Figs. 7a–7c.

The average roughness of polished carbon steel in 1.0 M HCl without inhibitor (Fig. 7a) was calculated to be 306.51 nm. It is clearly shown in Fig. 7a that the surface of carbon steel has a considerably porous structure with large and deep pores due to the acid attack on carbon steel surface. However in the presence of $1.0 \times 10^{-3}$ M concentration of DfS and DfMeO the average roughness were reduced to 199.81 and 162.20 nm, respectively, which indicate that the corrosion rate decreases due to the adsorption of inhibitor molecules on surface of the mild steel. The surface is more smooth in the presence of inhibitors (Figs. 7b, 7c) [63].

The efficiency of inhibitors against the corrosion of MS in 1.0 M HCl can be explained on the basis of the number of adsorption sites, the distribution of the charge on the molecule, molecular size, the nature and surface charge of the metal and mode of interaction with the metal surface. Schiff bases investigated for inhibitor activity contain lone pair of electrons located on the oxygen atom, protonated imine group

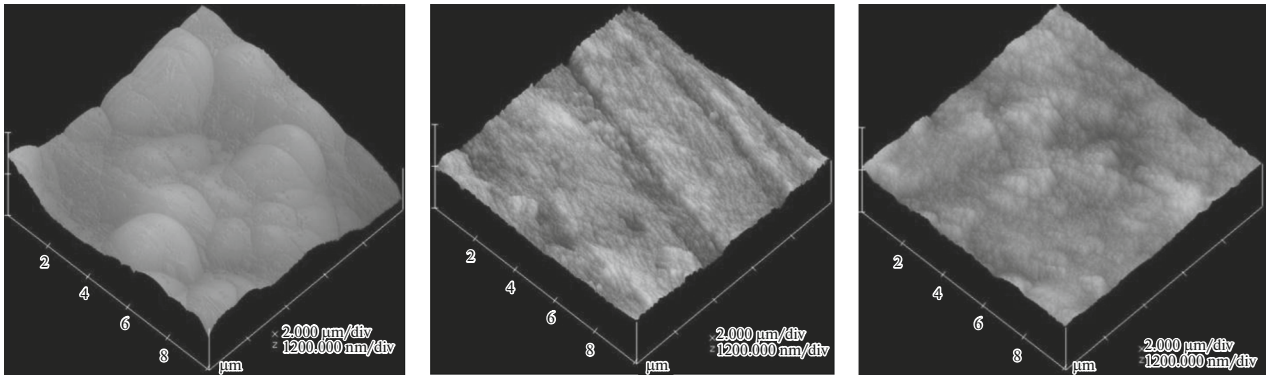


**Fig. 7.** AFM images of blank (a) and $1.0 \times 10^{-3}$ M DfS (b) and DfMeO (c) in 1.0 M HCl solution after immersion 120 h.

and delocalized π-electrons which act as adsorption centers. The protonated imine group can be bound physically to the positively charged mild steel surface through the negatively charge chloride ion (Cl). The electron configuration of iron is $[Ar]4s^2 3d^6$, the 3*d* orbitals are not fully filled with electrons. The oxygen atom has a lone pair of electrons as well as the π-electrons of the inhibitor molecule which can be donated to the *d*-orbital of Fe that form a coordinate type of a bond which enhances the combination intension between the inhibitor molecule and electrode surface [21, 37, 44, 64]. Two studied molecules act as good inhibitors for mild steel corrosion in 1.0 M HCl solution.The presence of electron releasing hydroxyl (OH) and methoxy ($OCH_3$) group in DfMeO, showed the higher inhibition efficiency as compared to inhibitor with only hydroxyl (OH) group in DfS.

## CONCLUSION

Corrosion inhibition of carbon steel in 1.0 M HCl solution by Schiff bases was studied. The main findings are as follows.

1. The Schiff bases show perfect inhibition efficiency for the corrosion of carbon steel in 1.0 M HCl solution. Inhibition efficiency was more pronounced with inhibitor concentration and temperature variables.

2. Schiff base compounds were found to be mixed-type inhibitors, affecting both anodic metal dissolution and cathodic proton reduction reactions.

3. The inhibitor molecule (DfMeO) having $OCH_3$ and OH groups exhibits the higher inhibition performance as compared to the inhibitor (DfS) having only OH group.

4. The Schiff bases are primarily physically adsorbed at lower concentrations, while strong physisorption is favored at higher concentrations. The adsorption of inhibitor molecules on the metal surface obey Langmiur adsorption isotherm.

5. Thermodynamic adsorption parameters such as $\Delta G^\circ_{ads}$, $\Delta H^\circ_{ads}$, and $\Delta S^\circ_{ads}$, show that inhibitors are adsorbed, and the adsorption process is a strong physical adsorption.

6. The morphology analysis together with the results obtained from electrochemical tests suggest that an ordered and dense protective layer could be formed by inhibitors.

## ACKNOWLEDGMENTS

We are thankful to the Scientific Research Projects Unit (NUBAP, project no. FEB 2012/29) of Nigde University for their financial support during this study.

## REFERENCES

1. R. A. Prabhu, T. V. Venkatesha, A. V. Shanbhag, G. M. Kulkarni, and R. G. Kalkhambkar, Corros. Sci. **50**, 3356 (2008).
2. L. A. Nnanna, I. O. Owate, O. C. Nwadiuko, N. D. Ekekwe, and W. J. Oji, Int. J. Mater. Chem. **3**, 10 (2013).
3. E. A. Noor and A. H. Al-Moubaraki, Mater. Chem. Phys. **110**, 145 (2008).
4. N. A. Negm, F. M. Ghuiba, and S. M. Tawfik, Corros. Sci. **53**, 3566 (2011).
5. N. Soltani, M. Behpour, S. M. Ghoreishi, and H. Naeimi, Corros. Sci. **52**, 1351 (2010).
6. G. Quartarone, L. Ronchin, A. Vavasori, C. Tortato, and L. Bonaldo, Corros. Sci. **64**, 82 (2012).
7. K. Sayın, H. Jafari, and F. J. Mohsenifa, Taiwan Inst. Chem. Eng. **68**, 43 (2016).
8. H. Keles, M. Keleş, I. Dehri, and O. Serindag, Mater. Chem. Phys. **112**, 173 (2008).
9. E. Bayol, K. Kayakırılmaz, and M. Erbil, Mater Chem. Phys. **104**, 74 (2007).
10. K. S. Jacob and G. Parameswaran, Corros. Sci. **52**, 224 (2010).
11. N. A. Negm, E. A. Badr, I. A. Aiad, M. F. Zaki, and M. M. Said, Corros. Sci. **65**, 77 (2012).
12. H. Ju, Zhen-Peng Kai, and Y. Li, Corros. Sci. **50**, 865 (2008).
13. M. Behpour, S. M. Ghoreishi, M. Salavati-Niasari, and B. Ebrahimi, Mater. Chem. Phys. **107**, 153 (2008).

14. I. Ahamad, R. Prasad, and M. A. Quraishi, Corros. Sci. **52**, 933 (2010).
15. R. Solmaz, E. Altunbas, and G. Kardas, Mater. Chem. Phys. **125**, 796 (2011).
16. M. Behpour, S. M. Ghoreishi, N. Mohammadi, N. Soltani, and M. Salavati-Niasari, Corros. Sci. **52**, 4046 (2010).
17. H. Abd El-Lateef, A. M. Abu-Dief, L. H. Abdel-Rahman, E. C. Sañudo, N. J. Aliaga, and N. J. Alcalde, Electroanal. Chem. **743**, 120 (2015).
18. S. E. Nataraja, T. V. Venkatesha, K. Manjunatha, B. Poojary, M. K. Pavithra, and H. C. Tandon, Corros. Sci. **53**, 2651 (2011).
19. K. C. Emregül, E. Düzgün, and O. Atakol, Corros. Sci. **48**, 3243 (2006).
20. C. M. Goulart, A. Esteves-Souza, C. A. Martinez-Huitle, C. J. F. Rodrigues, M. A. M. Maciel, and A. Echevarria, Corros. Sci. **67**, 281 (2013).
21. I. Danaee, O. Ghasemi, G. R. Rashed, M. Rashvand Avei, and M. H. Maddahy, J. Mol. Struct. **1035**, 247 (2013).
22. M. P. Desimone, G. Gordillo, and S. N. Simison, Corros. Sci. **53**, 4033 (2011).
23. M. A. Hegazy, A. M. Hasan, M. M. Emara, M. F. Bakr, and A. H. Youssef, Corros. Sci. **65**, 67 (2012).
24. N. F. Atta, A. M. Fekry, and H. M. Hassaneen, Int. J. Hydrogen Energy **36**, 6462 (2011).
25. H. Hamani, T. Douadi, D. Daoud, M. Al-Noaimi, R. A. Rikkouh, and S. Chafaa, J. Electroanal. Chem. **801**, 425 (2017).
26. B. S. Prathibha, H. P. Nagaswarupa, P. Kotteeswaran, and V. BheemaRaju, Mater. Today Proc. **4**, 12245 (2017).
27. R. Kumar, O. S. Yadav, and G. Singh, J. Mol. Liq. **237**, 413 (2017).
28. R. Kumar, H. Kimb, and G. Singh, J. Mol. Liq. **259**, 199 (2018).
29. N. O. Obi-Egbedi and I. B. Obot, Arabian J Chem. **6**, 211 (2013).
30. L. Herrag, B. Hammouti, S. Elkadiri, A. Aouniti, C. Jama, H. Vezin, and F. Bentiss, Corros. Sci. **52**, 3042 (2010).
31. A. Popova, Corros. Sci. **49**, 2144 (2007).
32. M. A. Hegazy, A. M. Badawi, S. S. Abd El Rehim, and W. M. Kamel, Corros. Sci. **69**, 110 (2013).
33. A. K. Singh, Sudhish K. Shuklaa, M. A. Quraishi, and E. E. Ebenso, J. Taiwan Inst. Chem. E **43**, 463 (2012).
34. H. Ashassi-Sorkhabi, B. Shaabani, and D. Seifzadeh, Appl. Surf. Sci. **239**, 154 (2005).
35. P. Muthukrıshnan, K. S. Kumar, B. Jeyaprabha, and P. Prakash, Metall. Mater. Trans. A **45**, 4510 (2014).
36. F. Mansfeld, J. Appl. Electrochem. **25**, 187 (1995).
37. S. S. A. Rehim, O. A. Hazzazi, M. A. Amin, and K. F. Khaled, Corros. Sci. **50**, 2258 (2008).
38. R. Solmaz, G. Kardas, M. Culha, B. Yazıcı, and M. Erbil, Electrochim. Acta **53**, 5941 (2008).
39. S. Deng, X. Li, and H. Fu, Corros. Sci. **53**, 760 (2011).
40. H. Keles, Mater. Chem. Phys. **130**, 1317 (2011).
41. J. Aljourani, K. Raeissi, and M. A. Golozar, Corros. Sci. **51**, 1836 (2009).
42. M. Behpour, S. M. Ghoreishi, N. Soltani, and M. Salavati-Niasari, Corros. Sci. **51**, 1073 (2009).
43. G. Avcı, Colloids Surf., A **317**, 730 (2008).
44. M. Erbil, Chim. Acta Turc. **1**, 59 (1988).
45. R. Solmaz, G. Kardas, B. Yazıcı, and M. Erbil, Colloid Surf., A **312**, 7 (2008).
46. H. Hamani, T. Douadi, D. Daouda, M. Al-Noaimi, R. A. Rikkouh, and S. J. Chafaa, Electroanal. Chem. **801**, 438 (2017).
47. A. M. Fekry and M. A. Ameer, Int. J. Hydrogen Energy **36**, 11207 (2011).
48. N. S. Ayati, S. Khandandel, M. Momeni, M. H. Moayed, A. Davoodi, and M. Rahimizadeh, Mater. Chem. Phys. **126**, 873 (2011).
49. F. Zhang, Y. Tang, Z. Cao, W. Jing, Z. Wu, and Y. Chen, Corros. Sci. **61**, 1 (2012).
50. M. Benabdellah, A. Tounsi, K. F. Khaled, and B. Hammouti, Arabian J. Chem. **4**, 17 (2011).
51. X. Li, S. Deng, and H. Fu, Corros. Sci. **55**, 280 (2012).
52. E. E. Oguzie, G. N. Onuoha, and A. I. Onuchukwu, Mater. Chem. Phys. **89**, 305 (2005).
53. M. S. Morad, Corros. Sci. **50**, 436 (2008).
54. R. Hasanov, M. Sadıkoğlu, and S. Bilgiç, Appl. Surf. Sci. **253**, 3913 (2007).
55. T. Ibrahim, H. Alayan, and Y. Al Mowaqet, Prog. Org. Coat. **75**, 456 (2012).
56. D. Seifzadeh, H. Basharnavaz, and A. Bezaatpour, Mater. Chem. Phys. **138**, 794 (2013).
57. M. M. Solomon, S. A. Umoren, I. I. Udosoro, and A. P. Udoh, Corros. Sci. **52**, 1317 (2010).
58. M. A. Amin, M. A. Ahmed, H. A. Arida, T. Arslan, M. Saracoglu, and F. Kandemirli, Corros. Sci. **53**, 540 (2011).
59. L. Li, Q. Qu, W. Bai, F. Yang, Y. Chen, S. Zhang, and Z. Ding, Corros. Sci. **59**, 249 (2012).
60. M. Bouklah, N. Benchat, B. Hammouti, A. Aouniti, and S. Kertit, Mater. Lett. **60**, 1901 (2006).
61. E. A. Flores, O. Olivares, N. V. Likhanova, M. A. Domínguez-Aguilar, N. Nava, D. Guzman-Lucero, and M. Corrales, Corros. Sci. **53**, 3899 (2011).
62. K. Tebbji, N. Faska, A. Tounsi, H. Oudda, M. Benkaddour, and B. Hammouti, Mater. Chem. Phys. **106**, 260 (2007).
63. E. Bayol, T. Gurten, A. A. Gurten, and M. Erbil, Mater. Chem. Phys. **112**, 624 (2008).
64. B G. E. Badr, Corros. Sci. **51**, 2529 (2009).